

## Two-dimensional topological nodal line semimetal in layered $X_2Y$ ( $X = \text{Ca, Sr, and Ba}$ ; $Y = \text{As, Sb, and Bi}$ )

Chengwang Niu,<sup>1,\*</sup> Patrick M. Buhl,<sup>1</sup> Gustav Bihlmayer,<sup>1</sup> Daniel Wortmann,<sup>1</sup> Ying Dai,<sup>2</sup>  
Stefan Blügel,<sup>1</sup> and Yuriy Mokrousov<sup>1</sup>

<sup>1</sup>*Peter Grünberg Institut and Institute for Advanced Simulation, Forschungszentrum Jülich and JARA, 52425 Jülich, Germany*

<sup>2</sup>*School of Physics, State Key Laboratory of Crystal Materials, Shandong University, 250100 Jinan, People's Republic of China*

(Received 7 February 2017; published 21 June 2017)

In topological semimetals the Dirac points can form zero-dimensional and one-dimensional manifolds, as predicted for Dirac/Weyl semimetals and topological nodal line semimetals, respectively. Here, based on first-principles calculations, we predict a topological nodal line semimetal phase in the two-dimensional compounds  $X_2Y$  ( $X = \text{Ca, Sr, and Ba}$ ;  $Y = \text{As, Sb, and Bi}$ ) in the absence of spin-orbit coupling (SOC) with a band inversion at the M point. A nontrivial  $\mathbb{Z}_2$  invariant of  $\mathbb{Z}_2 = 1$  remains although a tiny gap appears at the nodal line when SOC is included. The mirror symmetry as well as the electrostatic interaction, which can be engineered via strain, are responsible for the nontrivial phase. In addition, the nontrivial phase is further explicitly confirmed via the existence of exotic edge states without and with SOC.

DOI: [10.1103/PhysRevB.95.235138](https://doi.org/10.1103/PhysRevB.95.235138)

Topological semimetals (TSMs), as new topological states of matter in addition to topological insulators (TIs) [1,2] and topological crystalline insulators (TCIs) [3], have drawn enormous interest in recent years. Two prominent examples of TSMs are Dirac semimetals [4–10] and Weyl semimetals [11–18]. Their bulk states are gapless; conduction and valence bands touch only at discrete points in the Brillouin zone. The Dirac points in Dirac semimetals are composed of two Weyl points of opposite topological charge, which can be split by breaking either time-reversal symmetry or inversion symmetry, realizing so-called Weyl semimetals [11–18]. Like Dirac points in surface/edge states of TIs and TCIs, the set of Dirac (Weyl) points of Dirac (Weyl) semimetals is zero-dimensional. Recent work indicates that a set of Dirac points can also form a one-dimensional [19,20] ring in a class of TSMs called topological nodal line semimetals (TNLSs) [21–30], in which the conduction and valence bands touch along distinct “nodal” lines. Two kinds of definitions for the TNLSs are given according to the absence or presence of spin-orbit coupling (SOC) [31]. The existence of three-dimensional (3D) TNLS states has been confirmed for  $\text{PbTaSe}_2$  [30],  $\text{ZrSiS}$  [32], and  $\text{PtSn}_4$  [33].

To date, TIs and TCIs are realized in both 3D and two-dimensional (2D) systems [1–4]. 2D systems bear great potential for the investigation of exotic phenomena not available in 3D, such as the quantum spin or quantum anomalous Hall effects [34,35]. Recently, based on symmetry arguments it was shown that the 2D Dirac semimetals can also be symmetry-protected [36]. In this work, based on first-principles calculations, we report material realizations of TNLSs in a family of 2D materials,  $\text{Ca}_2Y$ ,  $\text{Sr}_2Y$ , and  $\text{Ba}_2Y$  ( $Y = \text{As, Sb, and Bi}$ ) triple layers, where the TNLS state is protected by the mirror symmetry  $z \rightarrow -z$ . The computed nonzero topological invariant and the emergent edge states demonstrate the TNLS phase clearly.

The density functional theory calculations are performed using the generalized gradient approximation (GGA) of Perdew-Burke-Ernzerhof (PBE) [37] for the exchange correlation potential as implemented in the FLEUR code [38] as well as in the Vienna *ab initio* simulation package (VASP) [39,40] for relaxation. For each configuration, the atomic positions and lattice parameters were optimized until the forces are smaller than 0.01 eV/Å with an energy cutoff of 500 eV. A 20 Å thick vacuum layer is used to avoid interactions between nearest slabs in VASP while the calculations are carried out with the film version of the FLEUR code [41]. From this the maximally localized Wannier functions (MLWFs) are constructed using the wannier90 code [42,43].

Bulk  $X_2Y$  compounds ( $X = \text{Ca, Sr, and Ba}$ ;  $Y = \text{As, Sb, and Bi}$ ) have tetragonal structure with space group  $I4/mmm$  and have already been synthesized experimentally [44,45]. As shown in Fig. 1(a), the crystal structure can be visualized as an alternating stacking of  $X(1)$  and  $X(2)/Y$  layers along the  $c$  axis.  $X(1)$  atoms are coplanar corresponding to  $D_{2h}$ -site symmetry, while the  $X(2)$  and  $Y$  atoms exhibit buckling with one of the two neighboring  $X(2)/Y$  layers translated by a vector  $(a/2 + b/2)$ . Investigations of the electronic structure of the bulk material show a two-dimensional character; i.e., the transport will be mainly in the in-plane direction (Fig. S1 in the Supplemental Material [46]). One  $X(1)$  layer and two  $X(2)/Y$  layers constitute the simplest thin film in an ideal stoichiometry  $X_2Y$ . For films with nonideal stoichiometry, additional bands are introduced around the Fermi level and band dispersions become quite complex (Fig. S2 in the Supplemental Material [46]). With ideal stoichiometry,  $X_2Y$ , total energy investigations show that the favorable triple-layer configuration consists of one  $X(1)$  layer enclosed by  $X(2)/Y$  layers, invariant under  $z \rightarrow -z$  reflection [see Fig. 1(a)]. For example, the  $z$ -reflection-symmetric  $\text{Ca}_2\text{As}$  trilayer is energetically more favorable by as much as 1.4 eV as compared to the structure with the  $\text{Ca}(1)$  layer on top of two  $\text{Ca}(2)\text{As}$  layers. We further confirm the stability of the  $\text{Ca}_2\text{As}$  trilayer by phonon calculations (Fig. S3 in the Supplemental Material [46]). The real phonon frequencies at

\*c.niu@fz-juelich.de

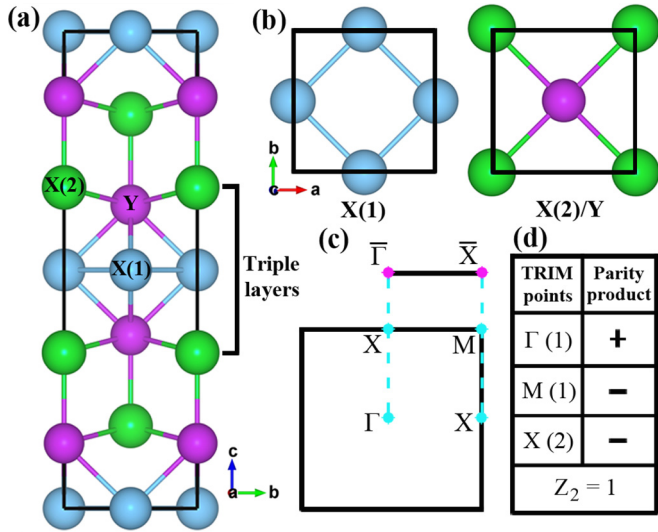


FIG. 1. (a) Bulk  $X_2Y$  ( $X = \text{Ca, Sr, and Ba}$ ;  $Y = \text{As, Sb, and Bi}$ ) crystallize in a tetragonal structure, space group  $I4/mmm$ , with the alternate stacking of  $X(1)$  and  $X(2)/Y$  layers. (b) Top view of  $X(1)$  (left) and  $X(2)/Y$  (right) layers. (c) Brillouin zone of the 2D triple layer and the projected 1D Brillouin zone. (d) Parity product of occupied states at TRIM points and the  $Z_2$  index for  $\text{Ca}_2\text{As}$ .

all momenta confirm that the proposed trilayer is dynamically stable.

To show the existence of Dirac nodal lines (DNLs) in  $X_2Y$  triple layers, we take  $\text{Ca}_2\text{As}$  as an example and analyze the projected band structure for this system without and with SOC

in Figs. 2(a) and 2(b), respectively. In the absence of SOC,  $\text{Ca}(2)-d_{(x^2-y^2)/z^2}$  and  $\text{Ca}(1)-d_{xy/yz/zx}$  orbitals overlap around the M point and the orbital characters exchange after passing through the band crossing points, indicating a band inversion with the  $\text{Ca}(1)-d_{xy/yz/zx}$  band being lower by 0.29 eV than the  $\text{Ca}(2)-d_{(x^2-y^2)/z^2}$  band. The gapless DNLs are realized as in the case of 3D  $\text{Ca}_3\text{PdN}$  [23,24] and Be [28] when SOC is ignored. The three-dimensional visualization of the nodal ring around the M point is presented in Fig. 2(c). Taking SOC into account, as shown in Fig. 2(b), band dispersion remains almost the same around the Fermi level, but a tiny splitting of the band crossing of about 2 meV is introduced (Fig. S4 in the Supplemental Material [46]).

The observed band inversion agrees well with the analysis of the topological  $Z_2$  invariant [23]. For a  $\text{Ca}_2\text{As}$  trilayer with space inversion symmetry, the parity eigenvalues at the four time-reversal-invariant momenta ( $\Gamma, 2X, M$ ) give the products  $\sigma_\Gamma = 1$  and  $\sigma_X = \sigma_M = -1$ , as shown in Fig. 1(d). This yields  $Z_2 = 1$  thus confirming the topologically nontrivial feature and an odd number of DNLs in the 2D Brillouin zone. The DNL is protected by the mirror symmetry  $z \rightarrow -z$ , and this mirror symmetry implies that, in the mirror plane, the two crossing bands can be classified in terms of the mirror eigenvalues  $\pm i$ . Figure 2(d) shows this clearly. Due to the presence of both time-reversal and inversion symmetries, the bands are degenerate when SOC is taken into account. The two crossing bands have opposite mirror eigenvalues in the vicinity of original crossing points although a tiny SOC-induced gap appears. The mirror-symmetry protection is further explicitly confirmed by the DNL that survives (without SOC) under a perturbation that keeps the mirror symmetry  $z \rightarrow -z$  while

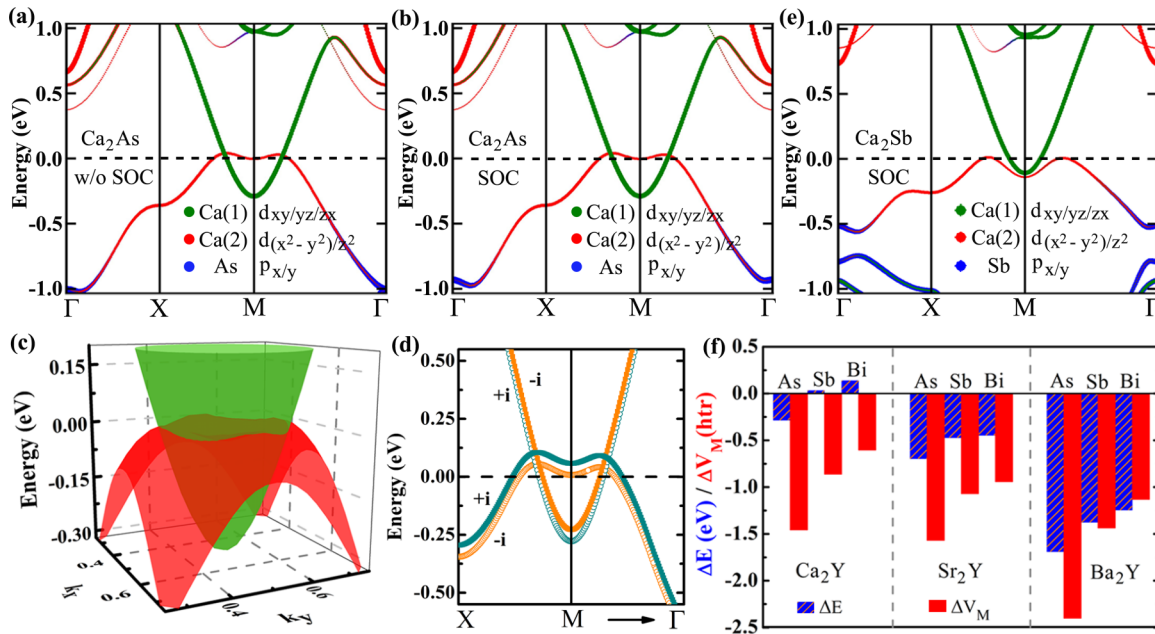


FIG. 2. Orbitaly resolved band structures for  $\text{Ca}_2\text{As}$  triple layers (a) without and (b) with SOC, weighted with the  $\text{Ca}(1)-d_{xy/yz/zx}$ ,  $\text{Ca}(2)-d_{(x^2-y^2)/z^2}$ , and  $\text{As}-p_{xy}$  characters. The band dispersions and the orbital contributions are almost the same in both cases, but a tiny gap is opened when SOC is included. (c) Band crossings of the bands near the Fermi level form a nodal line, which is protected by the mirror symmetry  $z \rightarrow -z$ , and (d) the bands can be assigned a mirror eigenvalue  $\pm i$  around the M point. Two pairs of crossing bands are denoted by solid squares and empty circles, respectively, and the solid squares have been shifted up by 50 meV for visibility. (e) Orbitaly resolved band structure of  $\text{Ca}_2\text{Sb}$  trilayer with SOC. A global gap appears around the M point. (f) Inversion energy  $\Delta E$  ( $\Delta E = E_{X(1)} - E_{X(2)}$ ) at the M point, and relative Madelung potential  $\Delta V_M$  ( $\Delta V_M = V_{X(1)} - V_{X(2)}$ ) for  $X_2Y$  trilayers.

it breaks the inversion and all kinds of rotational symmetries (Fig. S5 in the Supplemental Material [46]). In fact, similarly to topological crystalline insulators, a band gap in the system can be induced by breaking the crystal mirror symmetry. We demonstrate this by slightly moving Ca(2) and As atoms (by 0.46 Å) at one side of the layer along the  $z$  direction, and observing a gap opening at the original gapless crossing points (Fig. S6 in the Supplemental Material [46]). When considering the films consisting of an integer number of  $\text{Ca}_2\text{As}$  trilayers (Fig. S7 in the Supplemental Material [46]), we observed a nontrivial gap opening for an even number (when the mirror symmetry is broken), while the gapless DNLs survive for the odd number of the trilayers (when the mirror symmetry is preserved).

Similar nodal lines appear around the Fermi energy in  $\text{Sr}_2\text{Y}$  and  $\text{Ba}_2\text{Y}$ , but a global energy gap opens in  $\text{Ca}_2\text{Sb}$  and  $\text{Ca}_2\text{Bi}$  (Fig. S8 in the Supplemental Material [46]). In Fig. 2(e), which displays the projected band structure of  $\text{Ca}_2\text{Sb}$  including SOC, we observe that the lowest unoccupied bands are dominated by  $\text{Ca}(1)-d_{xy/yz/zx}$  states, while the highest occupied bands at the M point are dominated by the states of  $\text{Ca}(2)-d_{(x^2-y^2)/z^2}$  character. There is no band inversion around the M point in  $\text{Ca}_2\text{Sb}$  and  $\text{Ca}_2\text{Bi}$ , although they share the same lattice structure as well as symmetries with  $\text{Ca}_2\text{As}$ ,  $\text{Sb}_2\text{Y}$ , and  $\text{Ba}_2\text{Y}$ . This situation is analogous to typical TCIs such as the SnTe family [47], where SnTe is topologically nontrivial, while PbTe is a trivial insulator.

To investigate the origin of the DNLs in  $X_2Y$  further, we now focus on the role that the electrostatic interaction plays for their formation. Namely, we find that the energetic arrangement of the bands in this family relates directly to the electronegativity difference of the constituents  $\Delta\chi(X_2Y)$ ,  $\Delta\chi(X_2Y) = \chi(X) - \chi(Y)$ . Following the sequence  $|\Delta\chi(X_2\text{As})| > |\Delta\chi(X_2\text{Sb})| > |\Delta\chi(X_2\text{Bi})|$ , the inversion energy at the M point,  $\Delta E = E_{X(1)} - E_{X(2)}$ , increases and signals an inverted band arrangement at M when it is negative [see Fig. 2(f) and Table SI in the Supplemental Material [46]]. This trend explains the absence of the band inversions in  $\text{Ca}_2\text{Sb}$  and  $\text{Ca}_2\text{Bi}$  despite a stronger SOC of Bi and Sb atoms as compared to that of As. We further compute the Madelung potentials on  $X(1)$  ( $V_{X(1)}$ ) and  $X(2)$  ( $V_{X(2)}$ ) sites, whose contributions form the DNLs. We define the relative Madelung potential  $\Delta V_M$  as  $\Delta V_M = V_{X(1)} - V_{X(2)}$ . A clear correlation of the trend in  $\Delta E$  and  $\Delta V_M$ , presented in Fig. 2(f), indicates that the electrostatic interaction between  $X$  and  $Y$  atoms plays an important role for the band inversion as well as the formation of DNLs in the considered family of compounds, besides the mirror symmetry.

We further explore the stability of the band inversion with respect to strain, which is a very effective way to modulate the topological properties. Strain-induced phase transitions between normal insulators, TIs, and TCIs have been clearly confirmed [48–50]. The magnitude of the in-plane strain is described by the  $a/a_0$  ratio, where  $a_0$  and  $a$  denote the lattice parameters of the unstrained and strained systems, respectively. Internal atomic positions under homogeneous in-plane strain are fully relaxed. The corresponding As-Ca bond length  $d_{\text{As-Ca}}$ , inversion energy  $\Delta E$ , and relative Madelung potential  $\Delta V_M$  of  $\text{Ca}_2\text{As}$  versus the hydrostatic strain are

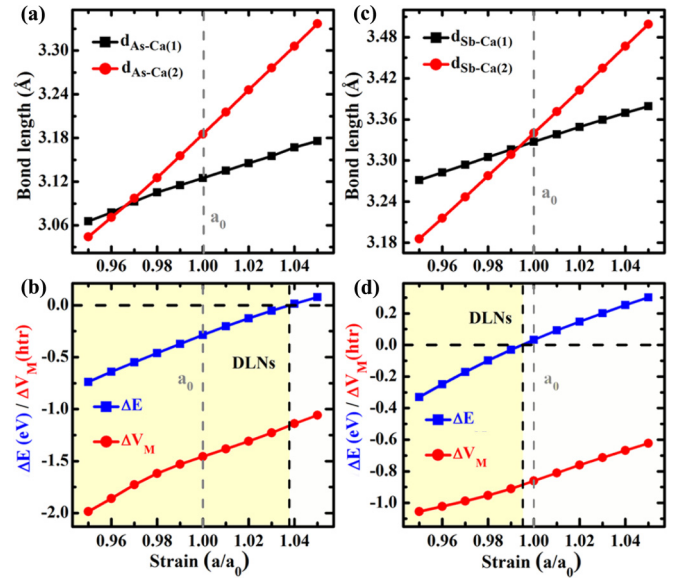


FIG. 3. Realization of a band inversion via strain for (a), (b)  $\text{Ca}_2\text{As}$  and (c), (d)  $\text{Ca}_2\text{Sb}$ . (a), (c) Bond lengths, (b), (d) inversion energy  $\Delta E$ , and relative Madelung potential  $\Delta V_M$  can be modulated effectively by hydrostatic strain with an accompanying phase transition between nontrivial and trivial semimetals. Negative  $\Delta E$  represents an inverted band and signals the emergence of a DNL around the M point.

presented in Figs. 3(a) and 3(b). As can be seen in this figure, all computed quantities are quite sensitive to strain. As the lattice parameters are increased, the As-Ca(1) and As-Ca(2) distances increase as well, resulting in a decreasing interaction between As and Ca states. However, as shown in Fig. 3(a),  $d_{\text{As-Ca}(2)}$  increases much faster than  $d_{\text{As-Ca}(1)}$ , and the variation of the corresponding Ca-As interaction is different for Ca(1) and Ca(2). This is clearly reflected in  $\Delta V_M$ , see Fig. 3(b). In the case of an increasing bond length both  $V_{X(1)}$  and  $V_{X(2)}$  decrease, but since  $V_{X(2)}$  changes more rapidly,  $\Delta V_M$  increases in accordance with  $\Delta E$  so that the DNLs disappear under tensile strain stronger than 3.8%. A similar trend is observed for  $\text{Ca}_2\text{Sb}$  [see Figs. 3(c) and 3(d)], for which the DNLs can be obtained by a compressive strain of about  $-0.5\%$ . In the latter case a strain-induced band inversion occurs at the M point due to the increase in the electrostatic interaction.

At this point, we are ready to demonstrate the emergence of characteristic edge states, which are another manifestation of the nontrivial topology of considered systems. Taking  $\text{Ca}_2\text{As}$  as an example, a symmetric nanoribbon with approximately 75 Å width with Ca(1)-As termination is constructed, and the dangling bonds of edge atoms are saturated by Li. The calculated band structures of the nanoribbon as well as projected bulk band structures are presented in Fig. 4. In the case without SOC, as shown in Fig. 4(a), one can easily see the emergence of topological edge states. Taking into account SOC, Fig. 4(b) shows that a SOC-induced spin splitting appears for the topological edge states, which cross each other at the  $\Gamma$  point and carry opposite spin polarizations. This is quite similar to surface/edge states of TIs.

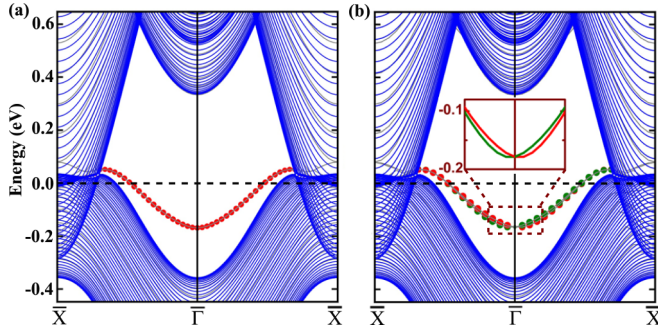


FIG. 4. Band structures of a  $\text{Ca}_2\text{As}$  nanoribbon with Ca(1)-As termination (gray lines) and the projected bulk band structure (blue lines) (a) without and (b) with SOC. Inset in panel (b) shows the zoom-in view at the  $\bar{\Gamma}$  point. The circle size denotes the weight of the outmost four layers at one edge and the color indicates the spin direction.

Finally, keeping the possibility for experimental observation in mind, we explore the possible realization of DNLs on a lattice-matching substrate and propose a quantum well structure which keeps the mirror symmetry in the system. For the  $\text{Ca}_2\text{As}$  trilayer, we select KCl films as cladding layers with a lattice mismatch of 3.9%. Figure 5(a) shows the orbitally resolved band structure of  $\text{Ca}_2\text{As}$  sandwiched between two KCl layers with optimized lattice constants in the absence of SOC. As can be seen, the energy bands with the Ca(2)- $d_{(x^2-y^2)/z^2}$  orbital character overlap around the M point with the Ca(1)- $d_{xy/yz/zx}$  states, in good qualitative agreement with freestanding  $\text{Ca}_2\text{As}$ . The crossing line of the conduction and valence bands in the 2D Brillouin zone is also explicitly shown in Fig. 5(b) in the vicinity of the M point. Similar to the freestanding  $\text{Ca}_2\text{As}$  trilayer, a tiny gap appears when SOC is taken into account. We also examine the feasibility of quantum well structure by calculating the interface formation energy, defined as  $2E_f = E_{\text{QW}} - E_{\text{Ca}_2\text{As}} - 2E_{\text{KCl}}$ , where  $E_{\text{QW}}$  is the total energy of the quantum well structure, while  $E_{\text{Ca}_2\text{As}}$  and  $E_{\text{KCl}}$  are the energies of thin films. The calculated interface formation energy for  $\text{Ca}_2\text{As}$  sandwiched between two KCl layers is  $E_f = -0.66$  eV, i.e., of a size comparable with the interface formation energy of two  $\text{Ca}_2\text{As}$  trilayers ( $-0.73$  eV). Thus a layered growth and the formation of a quantum well structure seems realistic. In addition, the DNL around the M point remains intact even though the KCl lattice parameters correspond to a 3.9% tensile strain (Fig. S9 in the Supplemental Material [46]). Remarkably, according to our calculations, we can state that the DNLs are obtained for a wide range of cladding layer thickness (Fig. S10 in the Supplemental

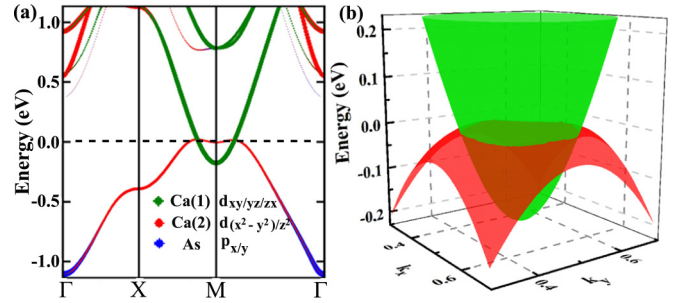


FIG. 5. (a) Orbitally resolved band structure of  $\text{Ca}_2\text{As}$  sandwiched between two KCl layers, weighted with the Ca(1)- $d_{xy/yz/zx}$ , Ca(2)- $d_{(x^2-y^2)/z^2}$ , and As- $p_{xy}$  characters. The band crossing remains even with the substrate present. (b) 3D representation of the band structure in (a) which shows the DNL around the M point.

Material [46]). We then consider the topologically trivial but isostructural  $\text{Ca}_2\text{Sb}$  as a substrate, which makes the proposed quantum well structure much easier to realize experimentally, and the DNL remains stable around the M point (Fig. S11 in the Supplemental Material [46]).

In summary, we theoretically predict that  $X_2Y$  ( $X = \text{Ca}, \text{Sr},$  and  $\text{Ba}$ ;  $Y = \text{As}, \text{Sb},$  and  $\text{Bi}$ ) triple layers realize a family of 2D topological nodal line semimetals protected by crystalline symmetry. A nonzero topological index and the emergence of the edge states demonstrate the nontrivial phase clearly. In addition, we reveal the possibility of the 2D topological nodal line semimetal states on a lattice-matching substrate. As various techniques have been developed to grow various 2D materials with complex structure, we expect that  $X_2Y$  trilayers and proposed quantum wells can be synthesized in experiments via molecular beam epitaxy and realize the 2D nontrivial phase presented above.

*Note added.* Recently, we became aware of three independent works on the prediction of  $\text{Hg}_3\text{As}_2$  [51], PdS [52], and  $\text{Be}_2\text{C}$  [53] as 2D TNLSs without SOC.

We are grateful for helpful discussions with J.-W. Rhim. This work was supported by the Priority Program 1666 of the German Research Foundation (Deutsche Forschungsgemeinschaft), the Virtual Institute for Topological Insulators (VITI), the National Basic Research Program of China (973 program, 2013CB632401), and the Taishan Scholar Program of Shandong Province. We acknowledge computing time on the supercomputers JUQUEEN and JURECA at the Jülich Supercomputing Centre and JARA-HPC of the RWTH Aachen University.

- [1] M. Z. Hasan and C. L. Kane, *Rev. Mod. Phys.* **82**, 3045 (2010).
- [2] X.-L. Qi and S.-C. Zhang, *Rev. Mod. Phys.* **83**, 1057 (2011).
- [3] Y. Ando and L. Fu, *Annu. Rev. Condens. Matter Phys.* **6**, 361 (2015).
- [4] Z. Wang, Y. Sun, X.-Q. Chen, C. Franchini, G. Xu, H. Weng, X. Dai, and Z. Fang, *Phys. Rev. B* **85**, 195320 (2012).
- [5] Z. Wang, H. Weng, Q. Wu, X. Dai, and Z. Fang, *Phys. Rev. B* **88**, 125427 (2013).

- [6] Z. K. Liu, B. Zhou, Y. Zhang, Z. J. Wang, H. M. Weng, D. Prabhakaran, S.-K. Mo, Z. X. Shen, Z. Fang, X. Dai, Z. Hussain, and Y. L. Chen, *Science* **343**, 864 (2014).
- [7] M. Neupane, S.-Y. Xu, R. Sankar, N. Alidoust, G. Bian, C. Liu, I. Belopolski, T.-R. Chang, H.-T. Jeng, H. Lin, A. Bansil, F. Chou, and M. Z. Hasan, *Nat. Commun.* **5**, 3786 (2014).
- [8] S. Borisenko, Q. Gibson, D. Evtushinsky, V. Zabolotnyy, B. Büchner, and R. J. Cava, *Phys. Rev. Lett.* **113**, 027603 (2014).

- [9] Z. K. Liu, J. Jiang, B. Zhou, Z. J. Wang, Y. Zhang, H. M. Weng, D. Prabhakaran, S.-K. Mo, H. Peng, P. Dudin, T. Kim, M. Hoesch, Z. Fang, X. Dai, Z. X. Shen, D. L. Feng, Z. Hussain, and Y. L. Chen, *Nat. Mater.* **13**, 677 (2014).
- [10] S. Jeon, B. B. Zhou, A. Gyenis, B. E. Feldman, I. Kimchi, A. C. Potter, Q. D. Gibson, R. J. Cava, A. Vishwanath, and A. Yazdani, *Nat. Mater.* **13**, 851 (2014).
- [11] X. Wan, A. M. Turner, A. Vishwanath, and S. Y. Savrasov, *Phys. Rev. B* **83**, 205101 (2011).
- [12] A. A. Burkov and L. Balents, *Phys. Rev. Lett.* **107**, 127205 (2011).
- [13] G. Xu, H. Weng, Z. Wang, X. Dai, and Z. Fang, *Phys. Rev. Lett.* **107**, 186806 (2011).
- [14] S.-M. Huang, S.-Y. Xu, I. Belopolski, C.-C. Lee, G. Chang, B. Wang, N. Alidoust, G. Bian, M. Neupane, C. Zhang, S. Jia, A. Bansil, H. Lin, and M. Z. Hasan, *Nat. Commun.* **6**, 7373 (2015).
- [15] H. Weng, C. Fang, Z. Fang, B. A. Bernevig, and X. Dai, *Phys. Rev. X* **5**, 011029 (2015).
- [16] S.-Y. Xu, I. Belopolski, N. Alidoust, M. Neupane, G. Bian, C. Zhang, R. Sankar, G. Chang, Z. Yuan, C.-C. Lee, S.-M. Huang, H. Zheng, J. Ma, D. S. Sanchez, B. Wang, A. Bansil, F. Chou, P. P. Shibayev, H. Lin, S. Jia, and M. Z. Hasan, *Science* **349**, 613 (2015).
- [17] B. Q. Lv, H. M. Weng, B. B. Fu, X. P. Wang, H. Miao, J. Ma, P. Richard, X. C. Huang, L. X. Zhao, G. F. Chen, Z. Fang, X. Dai, T. Qian, and H. Ding, *Phys. Rev. X* **5**, 031013 (2015).
- [18] L. X. Yang, Z. K. Liu, Y. Sun, H. Peng, H. F. Yang, T. Zhang, B. Zhou, Y. Zhang, Y. F. Guo, M. Rahn, D. Prabhakaran, Z. Hussain, S.-K. Mo, C. Felser, B. Yan, and Y. L. Chen, *Nat. Phys.* **11**, 728 (2015).
- [19] A. P. Schnyder and S. Ryu, *Phys. Rev. B* **84**, 060504(R) (2011).
- [20] T. T. Heikkilä and G. E. Volovik, *JETP Lett.* **93**, 59 (2011).
- [21] H. Weng, Y. Liang, Q. Xu, R. Yu, Z. Fang, X. Dai, and Y. Kawazoe, *Phys. Rev. B* **92**, 045108 (2015).
- [22] L. S. Xie, L. M. Schoop, E. M. Seibel, Q. D. Gibson, W. Xie, and R. J. Cava, *APL Mater.* **3**, 083602 (2015).
- [23] Y. Kim, B. J. Wieder, C. L. Kane, and A. M. Rappe, *Phys. Rev. Lett.* **115**, 036806 (2015).
- [24] R. Yu, H. Weng, Z. Fang, X. Dai, and X. Hu, *Phys. Rev. Lett.* **115**, 036807 (2015).
- [25] K. Mullen, B. Uchoa, and D. T. Glatzhofer, *Phys. Rev. Lett.* **115**, 026403 (2015).
- [26] Y. Chen, Y.-M. Lu, and H.-Y. Kee, *Nat. Commun.* **6**, 6593 (2015).
- [27] M. Zeng, C. Fang, G. Chang, Y.-A. Chen, T. Hsieh, A. Bansil, H. Lin, and L. Fu, [arXiv:1504.03492](https://arxiv.org/abs/1504.03492).
- [28] R. Li, X. Cheng, M. Hui, S. Wang, D. Li, Z. Zhang, Y. Li, and X.-Q. Chen, *Phys. Rev. Lett.* **117**, 096401 (2016).
- [29] G. Bian, T.-R. Chang, H. Zheng, S. Velury, S.-Y. Xu, T. Neupert, C.-K. Chiu, S.-M. Huang, D. S. Sanchez, I. Belopolski, N. Alidoust, P.-J. Chen, G. Chang, A. Bansil, H.-T. Jeng, H. Lin, and M. Z. Hasan, *Phys. Rev. B* **93**, 121113(R) (2016).
- [30] G. Bian, T.-R. Chang, R. Sankar, S.-Y. Xu, H. Zheng, T. Neupert, C.-K. Chiu, S.-M. Huang, G. Chang, I. Belopolski, D. S. Sanchez, M. Neupane, N. Alidoust, C. Liu, B. Wang, C.-C. Lee, H.-T. Jeng, C. Zhang, Z. Yuan, S. Jia, A. Bansil, F. Chou, H. Lin, and M. Z. Hasan, *Nat. Commun.* **7**, 10556 (2016).
- [31] C. Fang, Y. Chen, H.-Y. Kee, and L. Fu, *Phys. Rev. B* **92**, 081201(R) (2015).
- [32] L. M. Schoop, M. N. Ali, C. Straer, A. Topp, A. Varykhalov, D. Marchenko, V. Duppel, S. S. P. Parkin, B. V. Lotsch, and C. R. Ast, *Nat. Commun.* **7**, 11696 (2016).
- [33] Y. Wu, L.-L. Wang, E. Mun, D. D. Johnson, D. Mou, L. Huang, Y. Lee, S. L. Bud'ko, P. C. Canfield, and A. Kaminski, *Nat. Phys.* **12**, 667 (2016).
- [34] R. Yu, W. Zhang, H. Zhang, S. Zhang, X. Dai, and Z. Fang, *Science* **329**, 61 (2010).
- [35] C. Fang, M. J. Gilbert, and B. A. Bernevig, *Phys. Rev. Lett.* **112**, 046801 (2014).
- [36] S. M. Young and C. L. Kane, *Phys. Rev. Lett.* **115**, 126803 (2015).
- [37] J. P. Perdew, K. Burke, and M. Ernzerhof, *Phys. Rev. Lett.* **77**, 3865 (1996).
- [38] See <http://www.flapw.de>.
- [39] G. Kresse and J. Hafner, *Phys. Rev. B* **47**, 558 (1993).
- [40] G. Kresse and J. Furthmüller, *Phys. Rev. B* **54**, 11169 (1996).
- [41] H. Krakauer, M. Posternak, and A. J. Freeman, *Phys. Rev. B* **19**, 1706 (1979).
- [42] A. A. Mostofi, J. R. Yates, Y. S. Lee, I. Souza, D. Vanderbilt, and N. Marzari, *Comput. Phys. Commun.* **178**, 685 (2008).
- [43] F. Freimuth, Y. Mokrousov, D. Wortmann, S. Heinze, and S. Blügel, *Phys. Rev. B* **78**, 035120 (2008).
- [44] W. B. Pearson, *Z. Kristallogr.* **171**, 23 (1985).
- [45] M. Martinez-Ripoll, A. Haase, and G. Brauer, *Acta Cryst. Sect. B* **29**, 1715 (1973).
- [46] See Supplemental Material at <http://link.aps.org/supplemental/10.1103/PhysRevB.95.235138> for lattice parameters, crystal structures, and band structures for various configurations.
- [47] T. H. Hsieh, H. Lin, J. Liu, W. Duan, A. Bansil, and L. Fu, *Nat. Commun.* **3**, 982 (2012).
- [48] S. Chadov, X. Qi, J. Kübler, G. H. Fecher, C. Felser, and S. C. Zhang, *Nat. Mater.* **9**, 541 (2010).
- [49] K. Yang, W. Setyawan, S. Wang, M. B. Nardelli, and S. Curtarolo, *Nat. Mater.* **11**, 614 (2012).
- [50] C. Niu, P. M. Buhl, G. Bihlmayer, D. Wortmann, S. Blügel, and Y. Mokrousov, *Nano Lett.* **15**, 6071 (2015).
- [51] J. L. Lu, W. Luo, X. Y. Li, S. Q. Yang, J. X. Cao, X. G. Gong, and H. J. Xiang, *Chin. Phys. Lett.* **34**, 057302 (2017).
- [52] Y. Jin, R. Wang, J. Zhao, C. Zheng, L.-Y. Gan, J. Liu, H. Xu, and S. Y. Tong, [arXiv:1608.05791](https://arxiv.org/abs/1608.05791).
- [53] B. Yang, X. Zhang, and M. Zhao, *Nanoscale* (2017), doi:[10.1039/C7NR00411G](https://doi.org/10.1039/C7NR00411G).